A systematic search at 1612 MHz for OH maser sources. I - Survey near the Galactic Centre

Baud, B.; Habing, H.J.; Matthews, H.E.; Winnberg, A.

1979, *Astron. Astrophys. Suppl.* **35**, 179-192.

A SYSTEMATIC SEARCH AT 1612 MHZ FOR OH MASER SOURCES I SURVEY NEAR THE GALACTIC CENTRE

B. BAUD and H.J. HABING
Sterrewacht, Huygens Laboratorium, Leiden, The Netherlands
H.E. MATTHEWS and A. WINNBERG
Max-Planck-Institut für Radioastronomie, Bonn, Federal Republic of Germany

Received October 24, 1977

An area of about 20 square degrees, asymmetrically placed with respect to the Galactic Centre, has been systematically surveyed for the 1612 MHz OH line. The observations were made with the Dwingeloo 25 m telescope, the 100 m telescope at Effelsberg and the NRAO 43 m telescope. Here we present only the Type II OH/IR emission sources detected. In total 43 such sources have been found, five of which were previously known.

Key words: OH emission – Type II OH/IR sources – Galactic Centre

1. INTRODUCTION

Recent surveys of 1612 MHz OH emission have revealed a large number of optically unidentified Type II OH/IR maser sources in the plane of the Galaxy (e.g. Caswell and Haynes 1975, Johansson *et al.* 1977a). Such sources show strong emission in the 1612 MHz transition of the ground rotational state of OH and sometimes weak main line emission (Wilson and Barrett 1972). The characteristic double-peaked emission profile with a velocity separation, ΔV, between the two peaks of ~ 30 km s^{-1} allows them to be easily identified. Because of the high brightness temperature of the maser emission the stronger ones may be seen throughout a large part of the Galaxy.

The strong concentration of Type II OH/IR sources to the galactic plane, as found in systematic surveys, suggests that many are situated at large distances. The association of some nearby maser sources with long period (Mira) variables, considered to be of intermediate population type or population II objects, and the general increase in the number of Type II OH/IR sources towards smaller longitudes, as found by Johansson *et al.* (1977b), indicate that there may be a concentration of such sources in the central part of the Galaxy.

We have searched for 1612 MHz emission around the Galactic Centre (G.C.) using both the Dwingeloo 25 m telescope and the 100 m telescope at Effelsberg. The Dwingeloo observations covered an area of $3° \times 4°$ around the G.C. with low sensitivity. With the 100 m telescope we surveyed with three times better sensitivity a narrow strip between $\ell = 358°$ and $\ell = 14$ and between $b = +0°.5$ and $b = -0°.5$. Upon discovery of several sources with high radial velocities we surveyed a similar area, more extended in latitude, with an increased velocity coverage using the NRAO[1] 43 m telescope at Green Bank. This telescope was later used again to confirm all Type II OH/IR sources found in the three surveys and to obtain a spectrum of each source with improved velocity resolution.

The survey observations and equipment are discussed in Section 2. Analysis of the observations and a description of the confirmatory observations is given in Section 3. Section 4 presents the sources and their spectra. Selection effects in the observations are finally discussed in Section 5. A detailed analysis of the results will be given in a forthcoming paper.

2. EQUIPMENT AND SURVEY OBSERVATIONS

Instrumental parameters for the three telescopes at 18 cm are listed in table 1. HPBW is the halfpower beamwidth; η_A is the aperture efficiency for a point source. S/T_A is the conversion factor from antenna temperature to flux density and T_{syst} is the system temperature measured on cold sky.

[1] The National Radio Astronomy Observatory is operated by Associated Universities, Inc., under contract with the National Science Foundation.

The surveys were carried out by making integrations on a grid of positions, covering several different areas. A summary of the areas surveyed is shown in figure 1 and listed with the relevant observational parameters in table 2. Column 1 of table 2 designates with a capital letter the area that has been observed with each telescope using different observing parameters. Column 2 gives the telescope used, while the surveyed range in galactic longitude and latitude is listed in columns 3 and 4. Areas G, H and J are not described in table 2 because they are somewhat irregular. Instead, they are shown only in figure 1. The spacing between gridpoints, $\Delta\theta$, is given in column 5. It is in most cases equal to the HPBW. The overall bandwidth and useful velocity coverage are in columns 6 and 7 respectively. The frequency and velocity resolution, using a uniform weighting function, are listed in columns 8 and 9, while the integration time spent on each gridpoint and the 3σ sensitivity limit are given in columns 10 and 11. The 3σ sensitivity limit refers to the actual value measured on most gridpoints. It is usually somewhat higher than that inferred from the system temperature on cold sky listed in table 1, because of the noise added by the galactic background radiation around the G.C. and by the relatively strong ground radiation often entering the first sidelobes. For spectrally unresolved features the sensitivity limit will be higher than the values listed in table 2. This will be discussed in Section 5.

All the velocities quoted in this paper are given with respect to the local standard of rest (lsr). The velocity of the Sun is assumed to be 20 km s^{-1} towards $RA = 18^{h}$, $Dec = +0°$ (epoch 1900.0). We will now turn to a description of the observations with each telescope.

DWINGELOO

The Dwingeloo observations of areas A and B were carried out in February and March 1975, using a closed-cycle helium-cooled parametric amplifier. The linearly-polarized feed was orientated perpendicular to the ground. Because the 1612 MHz emission of most Type II OH/IR sources is unpolarized, the use of a linearly polarized feed does not introduce a bias in the source detection. The 256-channel autocorrelation spectrometer was used in a frequency-switched mode, switching over 2.5 MHz, with a duty cycle of 30 seconds. The signal band was centered on $V = 0$ km s^{-1}, the reference band on $V = -465$ km s^{-1}. The signal was clipped in a one-bit mode. The system was calibrated continuously against a noise tube of well-known and constant temperature. The off-line reduction procedure yielded spectra calibrated in antenna temperature. A first order baseline, fitted to both ends of each spectrum, was subtracted. Near the G.C. such a procedure did not significantly improve the presentation of the data because of broad absorption lines in that direction due to the OH in molecular clouds.

EFFELSBERG

Observations with the 100 m telescope in Effelsberg were performed with a cooled dual channel receiver system, using two orthogonally-polarized feeds which were fixed with respect to the ground. They were oriented at 45° to the horizon. The 384-channel autocorrelation spectrometer was split into two equal sections, each receiving signal over the same bandwidth of 2.5 MHz, centered on $V = 0$ km s^{-1}. The output of both receiver sections was later added and averaged. The total power mode of operation was used, with a reference of six minutes duration after every 16 spectra, taken on the position $\ell = 4°$, $b = +4°$. The integration time on the grid positions was 1 minute. The signal and reference spectra were generally well balanced, and a baseline fit was unnecessary, except for spectra taken near the G.C.

Area D, E and F and a major part of area C were observed in March 1975; the latter area was completed in October 1976 and April 1977.

GREEN BANK

The survey observations in Green Bank with the NRAO 43 m telescope were carried out in December 1975. The measurements were made at the Cassegrain focus using an up-converter system operating in only one

channel. The aperture efficiency of the Cassegrain system is not well known but is measured to be $\simeq 10\%$ worse than that of the primary focus (Turner, private communication). We therefore adopt $S/T_A = 4.0$ Jy K^{-1}. The 384 channel autocorrelation receiver was divided into two sections of 192 channels, each covering a total bandwidth of 2.5 MHz but centered at different velocities. In the case of area G, close to the plane, the velocity coverage complemented that of the Effelsberg survey, making it possible to search for high velocity sources. Each of the two receiver sections had an overlap of 65 km s^{-1} with the Effelsberg observations. On areas H and J, the two receiver sections were arranged to cover a large velocity range symmetrically around $V=0$ km s^{-1}. They had a mutual overlap of 30 km s^{-1}. Observations were made in the total power mode, and a total of five references, taken throughout the observing run at $\ell = 4°$, $b = +4°$ for area G, and at $\ell = 20°$, $b = +20°$ for areas H and J, were used. The references were averaged and the result was used in the final analysis. This was done in order to reduce as far as possible the noise in the spectra. Baseline irregularities were eliminated with a sixth-order polynomial fitted to the whole baseline. In view of the narrowness of the 1612 MHz maser emission this is a permissible procedure.

3. ANALYSIS AND CONFIRMATORY OBSERVATIONS

The extent of the survey observations is summarized in figure 1, where all the areas, listed in table 2, are drawn in galactic coordinates. The corresponding capital letter (column 1 of table 2) is put in the lower left-hand corner of each area. The blank and hatched squares on the left denote the 3σ sensitivities, in Jy, of the correspondingly marked areas. Hatched circles represent the HPBW's of the three telescopes used.

The roughly L-shaped region around the G.C., consisting of areas A, C, D, G, H and J, is the most important one because all the new Type II OH/IR sources have been found within its boundaries. It has been surveyed with different sensitivity over different velocity intervals at any one position, in a sense that the sensitivity is halved at $|V| > 220$ km s^{-1}. This may introduce a bias against weak sources at high velocities. However, almost all sources were found within the velocity range of $|V| < 220$ km s^{-1} covered by the Dwingeloo and Effelsberg observations. Only two sources were discovered outside this velocity range. They are both more than five times stronger than the 3σ sensitivity limit (0.7 Jy) at those velocities. If the sources at high radial velocities have a powerlaw luminosity distribution (arguments for this assumption will be given in a forthcoming paper) we could extrapolate from the two strong sources so far discovered that there exist more than 30 sources outside the velocity range of -220 to $+220$ km s^{-1} stronger than the present sensitivity limit. Since no such sources were found we conclude that the two sources detected are unusual in their high radial velocity and that the majority of Type II OH/IR sources at small longitudes have $|V| < 220$ km s^{-1}. This conclusion is supported by recent further 1612 MHz observations around the G.C. with improved sensitivity and velocity coverage. Preliminary analysis of these data taken with the 100 m telescope has revealed no new sources with $|V| > 220$ km s^{-1}. Hence, because the velocity coverage of the observations at all positions spans a range from at least -220 to $+220$ km s^{-1}, we may consider the L-shaped region to have been sampled completely in radial velocity.

A spectrum for every gridpoint was plotted. In the case of the Green Bank observations we made separate plots for each receiver section. Each individual spectrum was then inspected by eye, searching for both emission and absorption. More than 100 independent features were found. In this paper we present only those sources with the typical emission characteristics of Type II OH/IR sources (Wilson and Barrett 1972).

Since we had no data on the other OH lines, the identification of Type II OH/IR sources was based on two criteria only: (1) candidate sources should have a profile that shows the characteristic double structure with steep outer edges and more gradual inner slopes; (2) the intensity of the emission in neighbouring gridpoints around the position of the source should decrease as expected for a point source. Only those sources that were visible in at least two adjacent gridpoints were accepted.

In August 1977 the sources that satisfied the above criteria were reobserved at 1612 MHz in order to confirm their identification as Type II OH/IR objects and to obtain a profile with better velocity resolution.

For these observations we again used the 43 m telescope at Green Bank with a cooled dual-channel 18-cm receiver at the prime focus. The stability of the receiver allowed a total power observing mode, with a reference spectrum taken daily at $\ell = 40°$, $b = +40°$. The autocorrelation receiver was used in the parallel mode, with both receivers centered on the same velocity. The orthogonally polarized signals from the two receivers were added and averaged. The total bandwidth was 625 kHz, resulting in a frequency resolution, after Hanning weighting, of 6.5 kHz or 1.2 km s^{-1}. In most cases the telescope was pointed at the positions determined by interpolation of intensities between neighbouring gridpoints of the survey observations. The accuracy of the positions thus obtained are usually better than 2′.4. An offset of 2′.4 from the centre of the 43 m telescope beam at 18 cm corresponds to an attenuation of $\sim 5\%$. For most sources the measured flux density may thus be underestimated by at most a few percent.

In some cases an improved position was needed before an accurate line profile could be obtained. This was required when several emission lines were seen at one position and the identification of a Type II OH/IR source was difficult. In such cases we observed a grid of 4 positions around the suspected source and determined the position of each individual emission feature. The features with coinciding positions within the error limits were considered to belong to the same source. A spectrum using a total bandwidth of 625 kHz was subsequently taken at the derived position.

A few weak sources, detected with the 100 m telescope and suspected to be of Type II OH/IR, could not be confirmed with the 43 m telescope, in most cases because of a strong baseline curvature due to the presence of strong and broad OH absorption by molecular clouds near the Galactic Centre. The observations with the 43 m telescope in regions of strong absorption gradients were generally more confused than the observations with the 100 m telescope, because of the larger beam of the former telescope.

4. THE TYPE II OH/IR SOURCES

In total we have found 43 sources which we identify with Type II OH/IR objects. Five of these were previously known. All sources are listed in table 3 in order of increasing galactic longitude. The first two columns denote the galactic coordinates l and b. The corresponding right ascension and declination, and their rms positional uncertainties appear in columns 3 and 4. The radial velocities of the low- and high-velocity emission peaks relative to the lsr. are given in column 5. Columns 6 and 7 list the peak flux densities $S_{6.5}$ (epoch 1977.6) of both emission peaks obtained from the figures and the rms uncertainty in the measurement. A value of $S/T_A = 3.6$ Jy K^{-1} was assumed for the 43 m prime focus 18 cm system. Column 8 denotes the flux density S_I, integrated over all velocities of each emission component. In those cases, where the emission extends over all velocities between the emission peaks, $S_I(LV)$ and $S_{II}(HV)$ were determined over all velocities below and above the mean velocity between the two peaks.

Figures 2 to 42 show the 1612 MHz spectra of the Type II OH/IR sources taken with the 43 m telescope in August 1977. All sources listed in table 3 are included except for OH 5.0+1.5 and OH 0.3−0.2, which were not observed with the 43 m telescope. These spectra appear in Kerr and Bowers (1974) and Baud *et al.* (1975) respectively.

Each spectrum has a velocity coverage of 92 km s^{-1}, and a resolution of 1.2 km s^{-1}. The large velocity coverage is necessary in order to trace the spectral baseline, which was not always at nominal zero due to either 1612 MHz absorption within the bandpass or a strong continuum background that is absent in the reference spectrum. For every source the output from the two receiver sections was analyzed separately in order to determine the linear polarization of the emission. In most cases the sources were practically unpolarized. Some sources are discussed individually below.

OH 358.1 + 0.1 (figure 2). The emission at −26 and −18 km s^{-1} is probably real, as well as the absorption at −4 km s^{-1}. This spectrum is an example of the confusion of features at 1612 MHz near the Galactic Centre. Observations with a smaller beam are necessary in order to spatially separate the individual emission and absorption features.

OH 359.5+1.3 and **OH 359.7+1.3** (figures 5 and 6). These OH/IR sources are separated by less than one HPBW of the 43 m telescope and are visible in both figures 5 and 6.

OH 359.8+2.6 (figure 7). The low velocity component of this source does not show the typical steep outer edge. It is considered to be a Type II OH/IR source because of its point-like behaviour and the shape of the high velocity component, with a steep outer edge and a more gradual inner slope.

OH 0.0−0.1 (figure 8). Strong absorption is present at velocities lower than +90 km s^{-1}. The low velocity component in this spectrum is rather weak. Earlier survey observations with the 100 m telescope were less confused by the absorption and showed the low velocity peak more clearly.

OH 0.1+5.1 (figure 9). This source was first discovered by Kerr and Bowers (1974). The peak flux density of both the low and high velocity components in now (1977.6) 0.6 of the flux density in 1973.5.

OH 0.1+0.1 (figure 10). The two emission peaks are superposed on a broad plateau of emission that extends to well outside the velocity range determined by the peaks. A similar kind of profile has been found by Andersson *et al.* (1974) in the 1667 MHz emission of the strong source OH 26.5+0.6, although there the emission outside the two peaks is less pronounced.

OH 0.3−0.0 (figure 11). The emission of the low velocity component is superposed on the broad absorption at +54 km s^{-1}. Wide band observations around the indicated position show that both velocity components have the same position, confirming the identification as a Type II OH/IR source.

OH 1.7−0.0 (figure 20). This source shows a broad plateau of emission. It cannot be ruled out that this is due to a curvature in the baseline.

OH 2.2−1.7 (figure 21). The emission feature at −100 km s^{-1} was discovered during the confirmatory observations. Its position is not well determined and it is not clear whether this feature is associated with **OH 2.2−1.7**

OH 2.6−0.5 (figure 23). Chaisson and Dickinson (1972) discovered this Type II OH/IR object near Hoffman source 39 (Hoffman *et al.* 1971). The peak flux density of both velocity components determined from the present observations differs by a factor of 1.5 compared with the earlier observations. Chaisson and Dickinson (1972) suggest that there may be broad band 1612 MHz absorption in the dirrection of OH 2.6−0.5, due to the presence of a diffuse foreground cloud. Our wide-band survey observations give an upper limit to any such absorption of 0.4 K antenna temperature.

OH 3.3−0.3 (figure 24). Both emission peaks show linear polarization of about 20%.

OH 3.9+0.0 and **OH 4.4+0.0** (figures 26 and 28). The emission between the two peaks may be due to baseline curvature.

OH 5.9−0.4 (figures 30a and 30b). This source is situated 1° south of the strong continuum source W28. The strong emission peak at −21 km s^{-1} was discovered by Coles and Rumsey (1970). It is weakly circularly polarized. Because of insufficient velocity coverage they did not detect the associated emission at +13 km s^{-1}. In figure 30a, the profile has been clipped at 4 Jy in order to show the latter emission more clearly. The contrast in shape between the irregular high velocity component and the smooth low velocity component (figure 30b) is remarkable.

OH 0.8+1.4 (figure 33). The flux densities (epoch 1977.6) for both emission peaks are 25% less than those measured at epoch 1973.5 by Kerr and Bowers (1974).

OH 9.6+0.4 and **OH 9.9—0.1** (figures 35 and 36). Both sources show emission everywhere between the two peaks. This may well be due to baseline curvature.

OH 11.3+0.0 and **OH 11.5+0.1** (figures 40 and 42). These sources are separated by 14′. The high velocity component of OH 11.5+0.1 and the low velocity component of OH 11.3+0.0 coincide in velocity and the latter is seriously confused with the emission of the former. To obtain an estimate of the low velocity component of OH 11.3+0.0, we subtracted the high velocity component of OH 11.5+0.1 from the profile taken at the position of OH 11.3+0.0, correcting for beam attenuation. The resulting profile (shown dotted in figure 40) represents the low velocity component of OH 11.3+0.0. Its shape is clearly indicative of a Type II OH/IR source. The ratio between the peak flux densities of both velocity components agrees well with the

ratio determined from the observations with the 100 m telescope, which are not hampered by confusion because of the smaller beam size.

OH 11.4 −0.1 (figure 41). This source lies close to the two sources discussed above. The emission at +64 and +98 km s^{-1} belong to those strong sources and should be disregarded.

5. SELECTION EFFECTS

Here we mention briefly the selection effects introduced by the choice of velocity coverage, spectral resolution and the variability of Type II OH/IR sources. In a following paper the completeness of the present survey will be discussed.

5.1 Velocity coverage and resolution

In a large-scale spectral line survey one has to make a compromise between velocity coverage and resolution. As can be seen from table 3 almost all sources of this survey lie well within the velocity range $|V|<220$ km s^{-1}. In Section III we have argued that this velocity range covers essentially all Type II OH/IR sources near the Galactic Centre. The velocity coverage of the observations therefore seems to be complete. However, we also found that objects with exceptional velocity do occur, although very rarely.

The velocity resolution can seriously affect the sensitivity limit for spectrally unresolved features. Inspection of the Type II OH/IR sources found by Johansson *et al.* (1977a) shows that many velocity components have a full width at half-intensity (FWHI) of less than 3 km s^{-1}. The minimum FWHI they find is about 1.5 km s^{-1}. With the velocity resolutions of 2.3 and of 2.9 km s^{-1} used in the survey phase of the present work, many such sources would have been unresolved, resulting in a lower observed peak antenna temperature.

Our sample of sources is therefore biased against weak sources that have narrow (<2 km s^{-1}) velocity components. We estimate that the sensitivity limit for the detection of such sources may be twice the value quoted in table 2.

5.2 Variability

Many, if not all, OH/IR stars show regular variable intensity of both velocity components, typically with periods of several hundred days and ratios of maximum to minimum 1612 MHz flux density of typically between 2 and 4 (Harvey *et al.* 1974). The detection of those sources that have a time averaged intensity comparable to the detection limit depends among others on the phase of their radio "light curve". We do not however expect that variability will result in any systematic bias in our sample, because of its stochastic character for a given sample of sources at a given time.

ACKNOWLEDGEMENTS

We would like to thank T. Cram, who helped us to get familiar with the NRAO 43 m telescope system. B.B. is supported by a grant from the Netherlands Organization for the Advancement of Pure Research (Z.W.O.). He would like to thank Z.W.O. and the Kerkhoven-Bosscha Foundation for providing financial support for his visits to NRAO. H.E.M. thanks the Royal Society, the Max-Planck-Institut für Physik und Astrophysik in Munich and the Humboldt Foundation for their financial support. The Dwingeloo telescope is operated by the Netherlands Foundation for Radioastronomy.

REFERENCES

Andersson, C., Johansson, L.E.B., Goss, W.M., Winnberg, A. and Rieu, N.O.: 1974, *Astron. Astrophys.* **30**, 475.
Baud, B., Habing, H.J., Matthews, H.E., O'Sullivan, J.D. and Winnberg, A.: 1975, *Nature,* **258**, 406.
Caswell, J.L. and Haynes, R.: 1975, *Monthly Notices Roy. Astron. Soc.* **173**, 659.
Chaisson, E.J. and Dickinson, D.F.: 1972, *Astrophys. Letters* **12**, 119.
Coles, W.A. and Rumsey, V.H.: 1970, *Astrophys. J.* **159**, 247.
Harvey, P.M., Bechis, K.B., Wilson, W.J. and Ball, J.A.: 1974, *Astrophys. J. Suppl.* **27**, 331.
Hoffman, W.F., Frederik, C.L. and Emery, R.J.: 1971, *Astrophys. J.* **170**, L89.
Johansson, L.E.B., Andersson, C., Goss, W.M. and Winnberg, A.: 1977a, *Astron. Astrophys. Suppl.* **28**, 199.
Johansson, L.E.B., Andersson, C., Goss, W.M. and Winnberg, A.: 1977b, *Astron. Astrophys.* **54**, 323.
Kerr, F.J. and Bowers, P.F.: 1974, *Astron. Astrophys.* **36**, 225.
Wilson, W.J. and Barrett, A.H.: 1972, *Astron. Astrophys.* **17**, 385.

B. Baud
H.J. Habing

Sterrewacht, Huygens Laboratorium
Wassenaarseweg 78
Leiden (The Netherlands)

H.E. Matthews
A. Winnberg

Max-Planck-Institut für Radioastronomie
Auf dem Hügel 69
D–53 Bonn (Federal Republic of Germany)

Table 1 Instrumental parameters

Telescope	HPBW (')	η_A	S/T_A (Jy K^{-1})	T_{syst} (K)
Dwingeloo	31	0.58	9.6	45
Effelsberg	7.7	0.49	0.7	60
Green Bank, Cassegrain*	18	0.49	4.0	65
Prime focus	18	0.54	3.6	60

* Turner (private communication).

Table 2 Survey parameters

Area	Telescope	Extent l	Extent b	$\Delta\theta$	Overall Bandwidth (MHz)	Radial Velocity range (km s^{-1})	Resolution (kHz)	Resolution (km s^{-1})	t (min)	3σ (Jy)
A	Dwingeloo	359°1 to 2°1	−2°1 to +2°1	0°3	2.5	−220 to +220	11.7	2.2	40	2.5
B	"	2.0 8.0	+2.0 +8.0	0.3	2.5	−220 +220	11.7	2.2	5	3.6
C	Effelsberg	358.0 14.0	−0.5 +0.5	0.125	2.5	−220 +220	15.6	2.9	1	0.3
D	"	359.5 1.0	+1.0 +1.75	0.125	2.5	−220 +220	15.6	2.9	1	0.3
E	"	359.5 0.25	+8.5 +9.25	0.125	2.5	−220 +220	15.6	2.9	1	0.3
F	"	0.25 1.75	+9.25 +10.0	0.125	2.5	−220 +220	15.6	2.9	1	0.3
G	Green Bank	see Figure 1		0.25	2.5	+167 +632	15.6	2.9	5	0.8
						−632 −167	15.6	2.9	5	0.8
H,J	"			0.25	2.5	−547 +547	15.6	2.9	5	0.7

Table 3 Type II OH/IR sources near the galactic centre

l	b	RA (1950)	DEC (1950)	V LV (km s^{-1})	V HV (km s^{-1})	$S_{6.5}$ LV (Jy)	$S_{6.5}$ HV (Jy)	ΔS_{rms} (Jy)	S_I LV (10^{-22} W m^{-2})	S_I HV (10^{-22} W m^{-2})	
358.06	+0.13	17^{h}37^m.2 ± 0.2	-30°30' ± 3	- 40	- 11	1.1	1.3	0.2	1.4	0.8	
359.1	+1.2	17 35.6 ± 1.7	-29 02 ± 25	-145	-127	1.8	1.6	0.1	1.9	1.8	
359.37	-1.25	17 45.8 ± 0.2	-30 06 ± 3	-234	-203	4.4	5.3	0.2	8.1	7.9	
359.54	+1.29	17 26.4 ± 0.1	-28 37 ± 1	+ 18	+ 45	1.6	0.4	0.1	1.8	0.9	
359.70	+1.25	17 36.9 ± 0.3	-28 30 ± 4	+ 33	+ 62	0.7	0.8	0.1	0.9	1.0	
359.75	+2.63	17 31.7 ± 0.1	-27 43 ± 2	+ 37	+ 60	4.7	5.3	0.1	10.2	9.9	
0.03	-0.13	17 43.0 ± 0.1	-28 58 ± 1	+ 99	+127	0.8	1.9	0.2	0.5	4.2	
0.1	+5.1	17 23.3	-26 03	-151	-135	2.6	1.1+	0.1	2.3	1.1	
0.14	+0.06	17 42.6 ± 0.1	-28 46 ± 1	+146	+174	2.0	3.1	0.2	11.1	11.9	
0.26	-0.01	17 43.1 ± 0.1	-28 42 ± 1	+ 58	+ 93	1.5	4.4	0.2	1.3	6.5	
0.330	-0.193	17 44.0 ± 0.03	-28 44.2 ± 0.4	-357	-328	4.9	3.4		8.0	7.8	x
0.38	+0.13	17 42.9 ± 0.2	-28 32 ± 3	+125	+155	1.0	0.9	0.2	1.1	1.2	
0.48	-0.13	17 44.1 ± 0.1	-28 35 ± 1	- 64	- 30	1.1	0.8	0.1	1.3	1.4	
0.5	-0.8	17 46.6 ± 1.1	-28 53 ± 17	+130	+154	0.9	1.4	0.1	1.5	1.9	
1.09	+0.38	17 43.6 ± 0.2	-27 47 ± 3	-143	-108	0.8	1.3	0.1	2.3	1.8	
1.10	-0.80	17 48.2 ± 0.2	-28 24 ± 3	- 9	+ 30	25.4	30.5	0.2	59.9	60.8	
1.21	+1.26	17 40.5 ± 0.1	-27 13 ± 1	+ 31	+ 58	5.6	5.3	0.2	6.0	5.5	
1.33	+1.01	17 41.7 ± 0.1	-27 15 ± 1	- 27	+ 3	4.2	4.2	0.2	8.4	5.4	
1.46	-0.01	17 46.0 ± 0.1	-27 41 ± 1	-141	-114	3.0	4.1	0.2	2.7	3.5	
1.74	-0.01	17 47.0 ± 0.1	-27 29 ± 1	+105	+134	0.8	4.2	0.2	4.7	8.5	
2.17	-1.65	17 54.0 ± 0.1	-27 55 ± 1	- 91	- 55	4.2	6.7	0.3	5.1	7.0	
2.50	+0.25	17 47.4 ± 0.3	-26 39 ± 5	- 86	- 71	0.4	0.5	0.1	0.3	0.4	
2.59	-0.45	17 50.3 ± 0.1	-26 56 ± 1	- 27	+ 19	6.1	7.2	0.2	11.2	14.3	xx
3.25	-0.28	17 51.1 ± 0.3	-26 17 ± 4	- 96	- 69	1.6	1.7	0.1	2.0	1.6	
3.25	+0.00	17 50.1 ± 0.3	-26 08 ± 5	- 57	- 25	1.2	1.5	0.1	1.3	2.9	
3.94	+0.00	17 51.6 ± 0.1	-25 33 ± 2	- 31	+ 1	1.2	1.1	0.1	2.7	2.6	
4.00	-0.50	17 53.7 ± 0.3	-25 45 ± 5	- 13	+ 10	0.8	0.4	0.1	2.3	0.9	
4.40	+0.01	17 52.6 ± 0.2	-25 09 ± 3	- 18	+ 16	3.2	1.2	0.1	5.4	2.1	
4.54	-0.38	17 54.4 ± 0.1	-25 13 ± 1	-144	-100	1.3	1.9	0.2	4.2	3.7	
5.0	+1.5	17 48.5	-23 50	+107	+135	5	4		3.2	2.5	++
5.90	-0.38	17 57.4 ± 0.1	-24 03 ± 1	- 21	+ 13	34.7	1.5	0.2	37.9	3.8	
6.00	+0.25	17 55.3 ± 0.1	-23 39 ± 2	+ 94	+106	1.8	1.3	0.2	1.8	1.2	
6.50	-0.13	17 57.8 ± 0.2	-23 24 ± 3	+ 93	+114	0.7	1.2	0.1	1.3	2.1	
8.0	+1.4	17 55.2	-21 20	- 34	- 9	4.2	6.6+	0.2	7.4	8.2	
9.00	-0.13	18 03.2 ± 0.2	-21 14 ± 3	-66	- 33	0.7	1.3	0.1	0.8	1.6	
9.63	+0.38	18 02.6 ± 0.1	-20 26 ± 2	-77	- 46	1.3	2.8	0.1	1.8	4.9	
9.88	-0.13	18 05.0 ± 0.3	-20 28 ± 5	+79	+112	1.9	0.8	0.1	4.0	1.8	
10.04	-0.10	18 05.2 ± 0.1	-20 19 ± 2	+23	+ 80	0.7	2.7	0.2	1.5	5.1	
10.38	+0.00	18 05.6 ± 0.2	-19 58 ± 3	+43	+ 79	0.6	0.8	0.2	0.5	2.2	
11.13	+0.00	18 07.1 ± 0.3	-19 19 ± 5	-35	- 8	0.9	1.1	0.1	0.8	0.7	
11.32	+0.00	18 07.5 ± 0.1	-19 09 ± 2	+64	+ 98	2.1	2.9	0.2	3.1	3.7	
11.38	-0.13	18 08.1 ± 0.3	-19 09 ± 5	+87	+123	0.5	0.4	0.1	0.6	0.9	
11.54	+0.10	18 07.6 ± 0.1	-18 54 ± 1	+20	+ 64	4.2	25.0	0.1	18.2	111.4	

\+ Previously known, position quoted from Kerr and Bowers (1974).

++ Previously known, all parameters quoted from Kerr and Bowers (1974).

x Previously known, all parameters quoted from Baud et al. (1975).

xx Previously known as OH 2.7 - 0.3 (Chaisson and Dickinson, 1972).

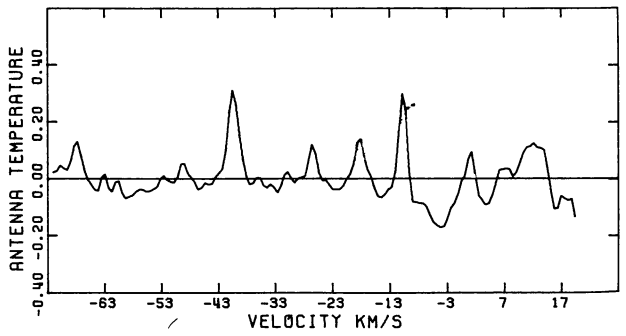

Figure 2 OH 358.1+0.1.

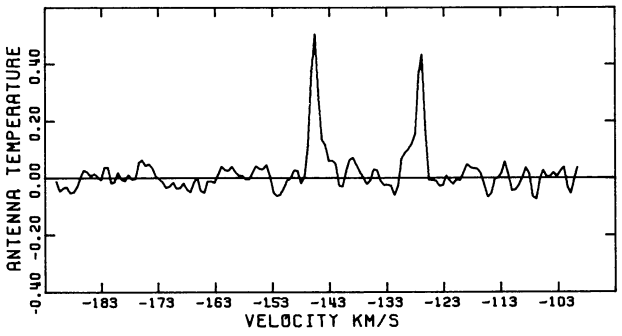

Figure 3 OH 359.1+1.2.

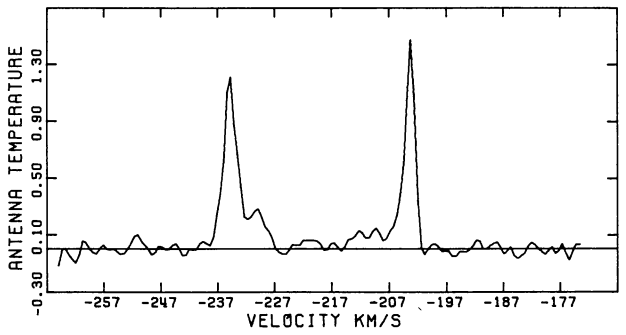

Figure 4 OH 359.4−1.3.

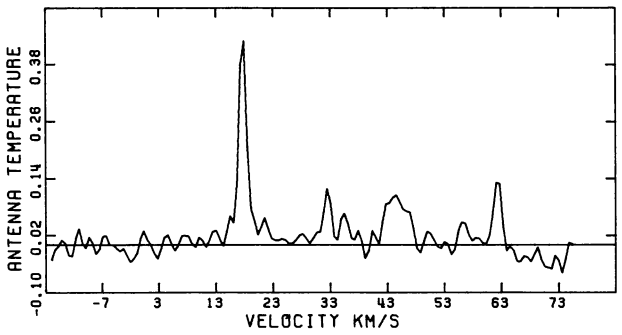

Figure 5 OH 359.5+1.3.

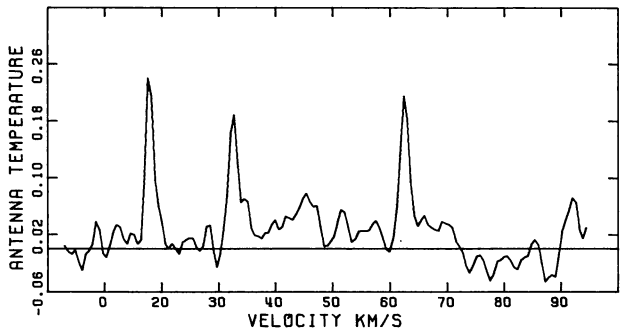

Figure 6 OH 359.7+1.3.

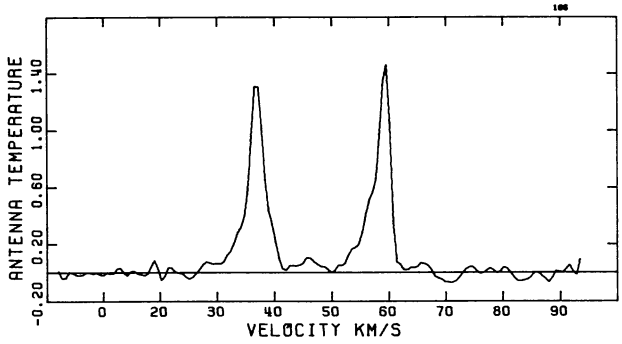

Figure 7 OH 359.8+2.6.

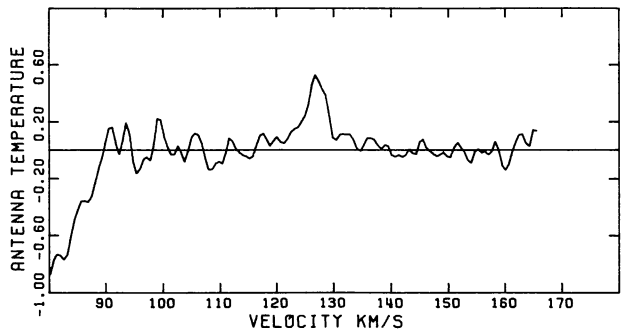

Figure 8 OH 0.0−0.1.

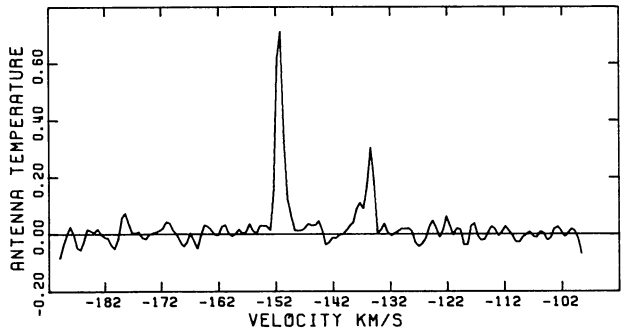

Figure 9 OH 0.1+5.1.

Figures 2 to 42 The 1612-MHz OH profiles of the sources in table 3. Antenna temperatures are given in degrees Kelvin. The velocity scale is with respect to the l.s.r. To convert to Janskys, multiply by 3.6.

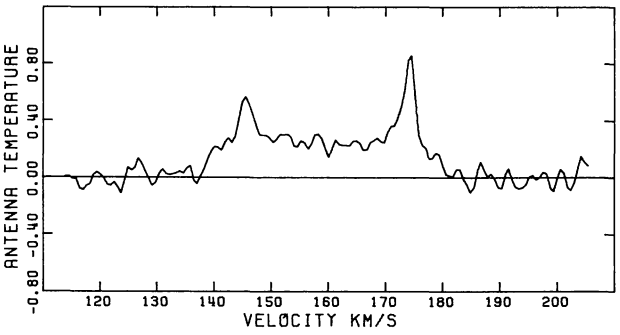

Figure 10 OH 0.1+0.1.

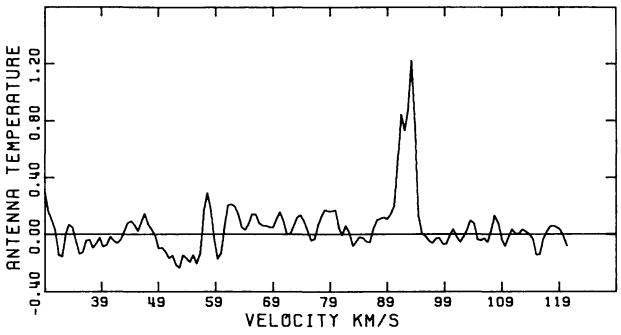

Figure 11 OH 0.3−0.0.

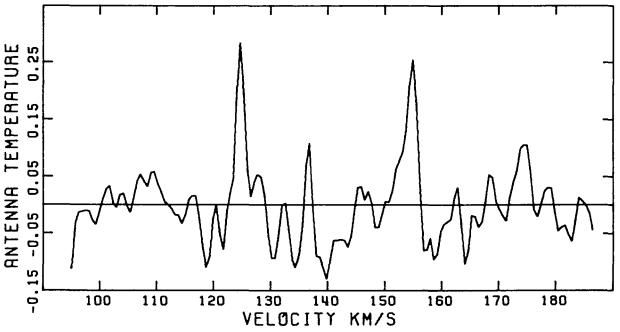

Figure 12 OH 0.4+0.1.

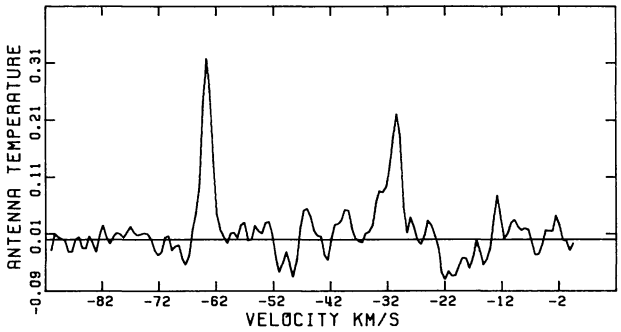

Figure 13 OH 0.5−0.1.

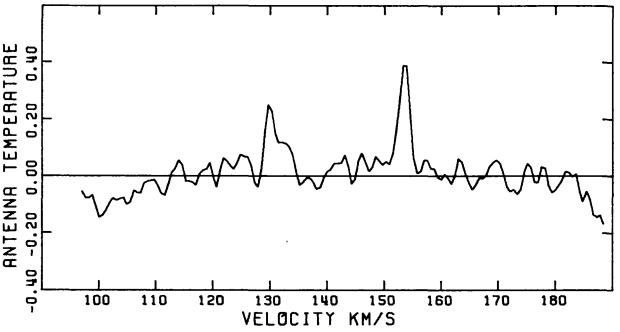

Figure 14 OH 0.5−0.8.

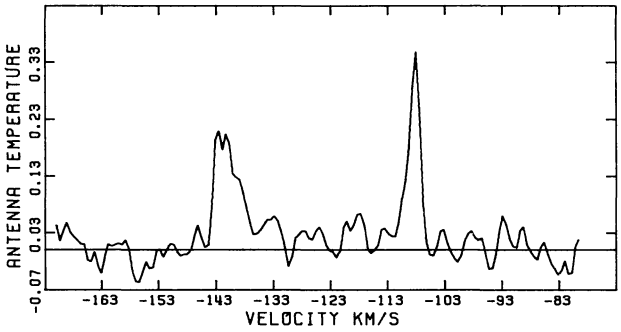

Figure 15 OH 1.1+0.4.

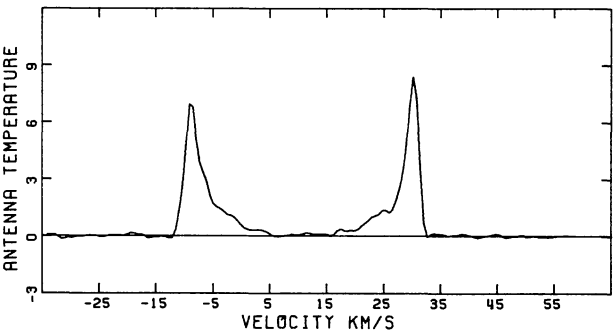

Figure 16 OH 1.1−0.8.

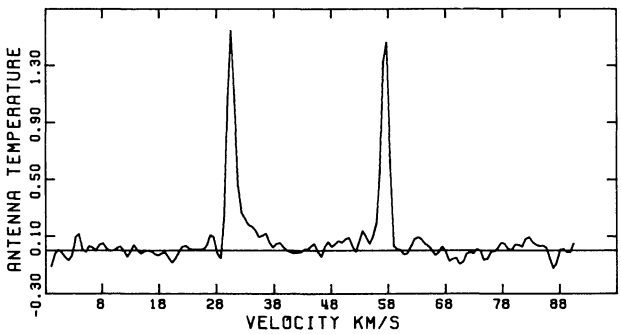

Figure 17 OH 1.2+1.3.

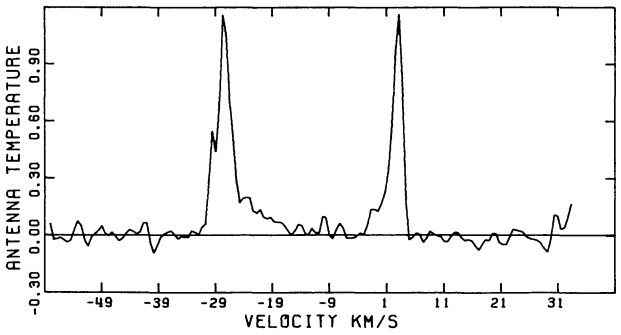

Figure 18 OH 1.3+1.0.

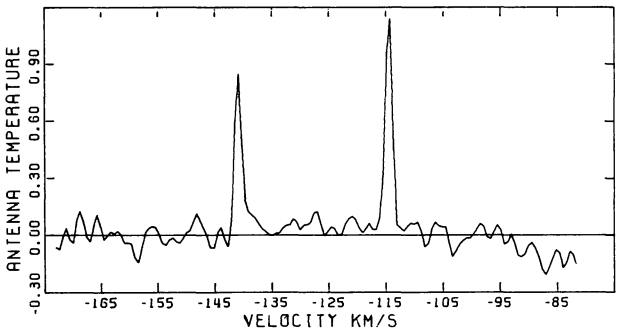

Figure 19 OH 1.5−0.0.

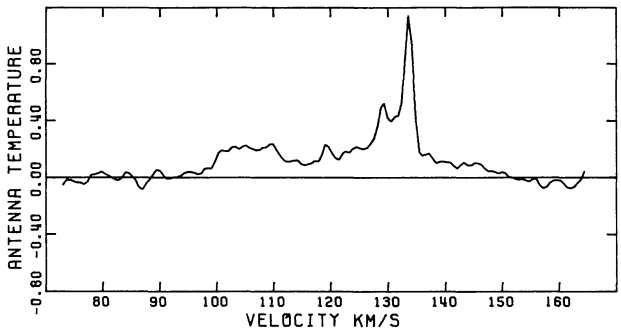

Figure 20 OH 1.7−0.0.

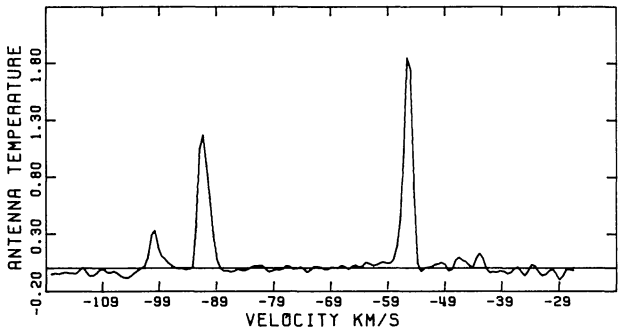

Figure 21 OH 2.2−1.7.

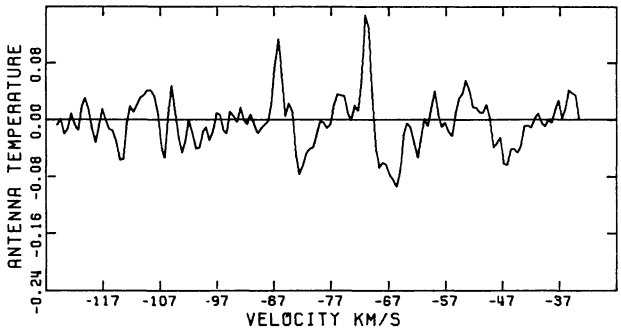

Figure 22 OH 2.5+0.3.

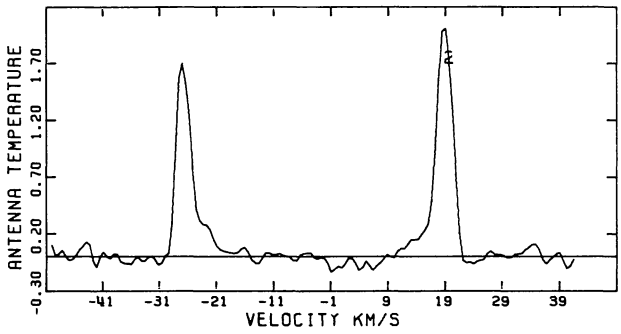

Figure 23 OH 2.6−0.5.

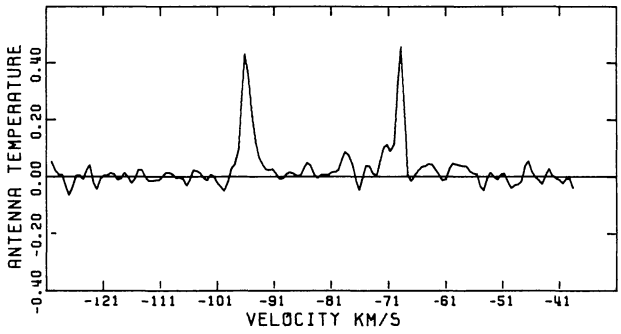

Figure 24 OH 3.3−0.3.

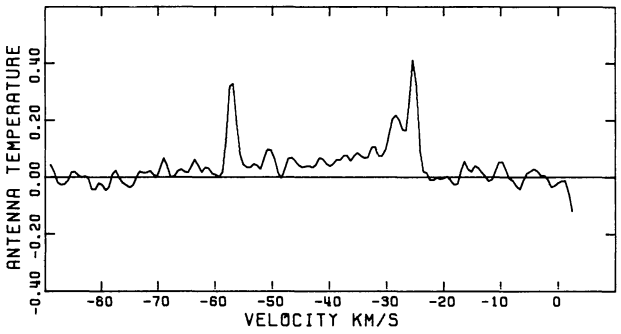

Figure 25 OH 3.3+0.0.

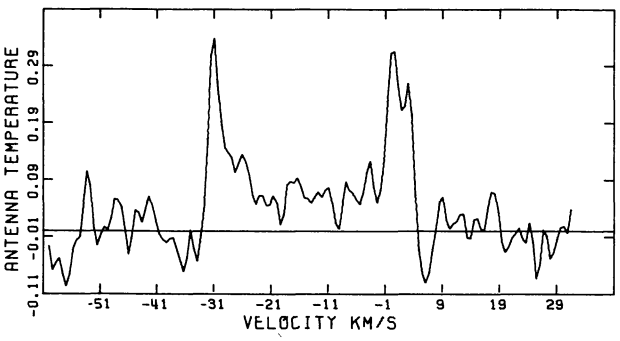

Figure 26 OH 3.9+0.0.

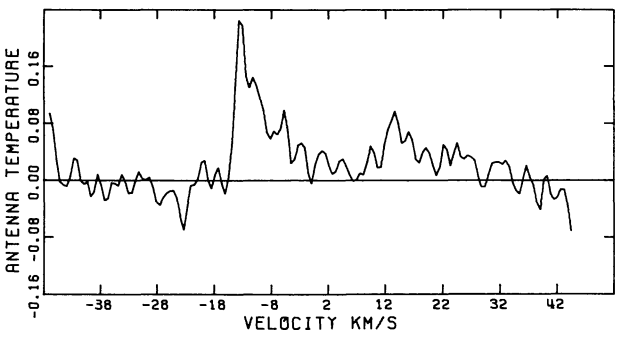

Figure 27 OH 4.0−0.5.

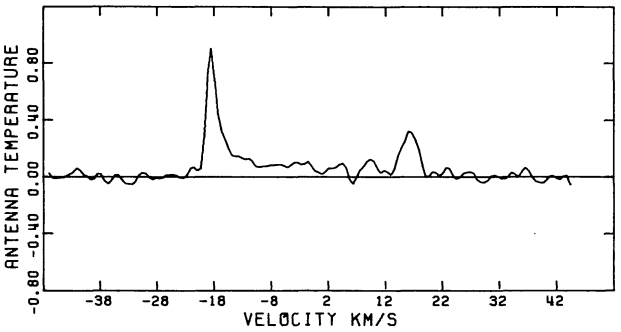

Figure 28 OH 4.4+0.0.

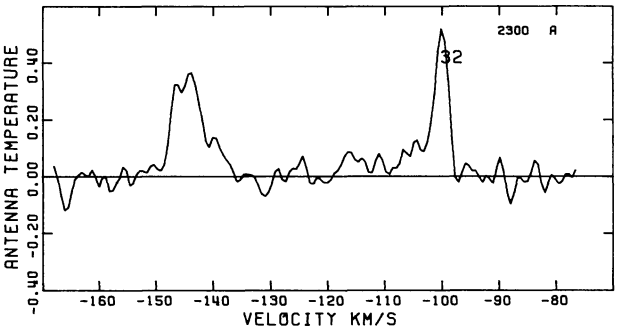

Figure 29 OH 4.5−0.4.

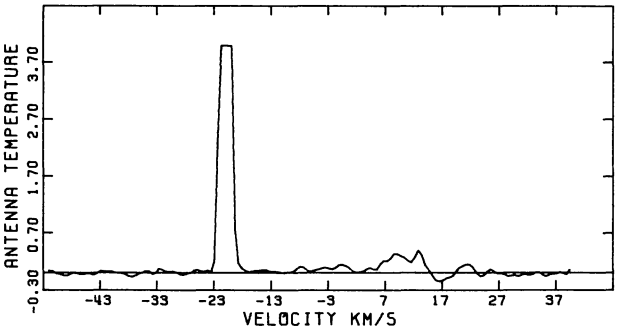

Figure 30a OH 5.9−0.4, profile is clipped at $T_A = 4$ K for a good representation of the high velocity component.

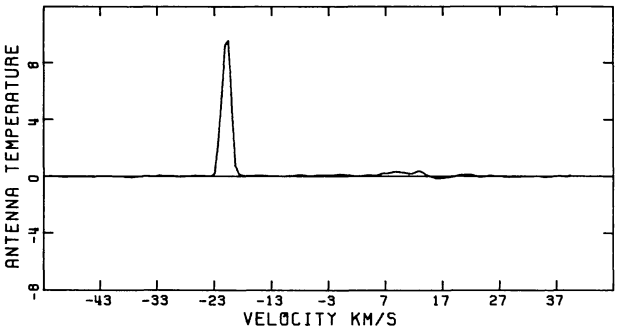

Figure 30b OH 5.9−0.4, profile is unclipped.

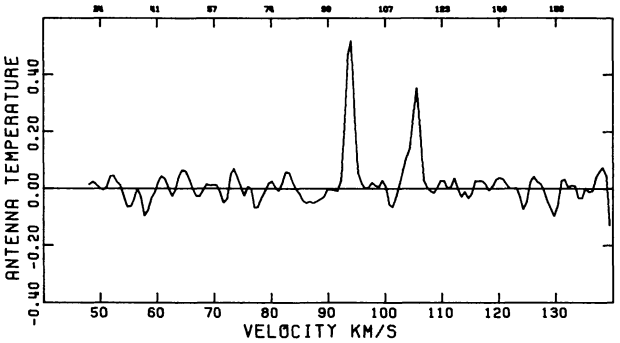

Figure 31 OH 6.0+0.3.

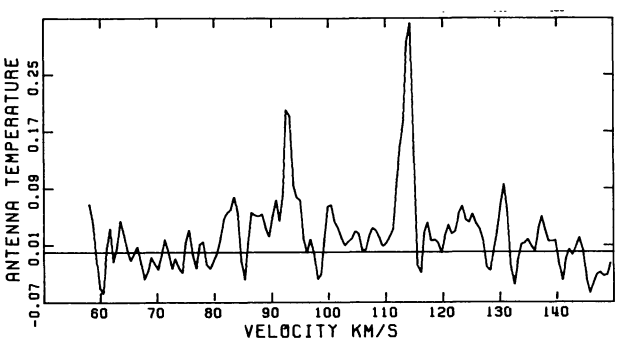

Figure 32 OH 6.5−0.1.

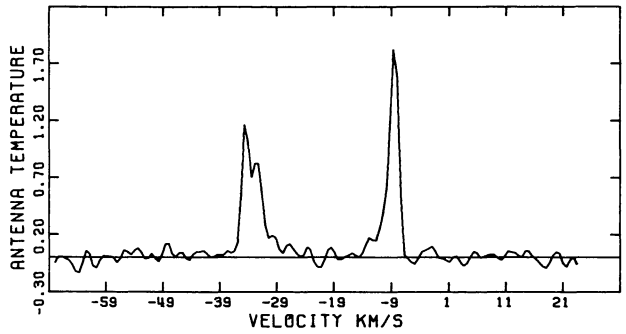

Figure 33 OH 8.0+1.4.

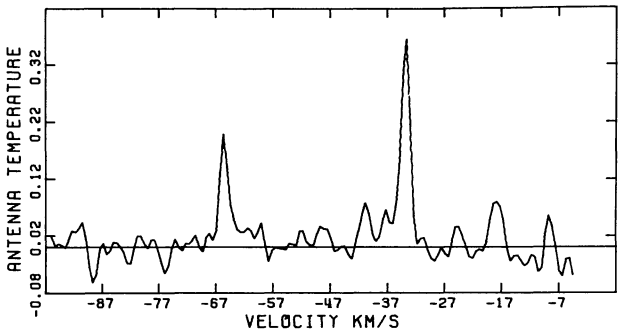

Figure 34 OH 9.0−0.1.

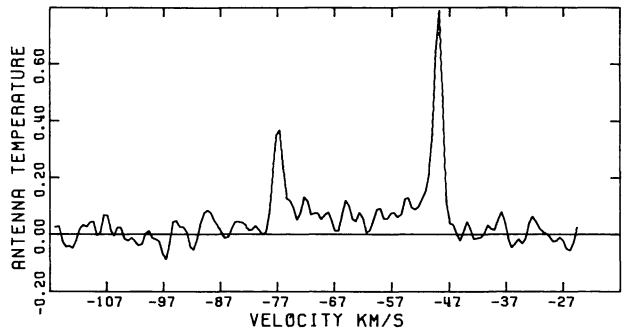

Figure 35 OH 9.6+0.4.

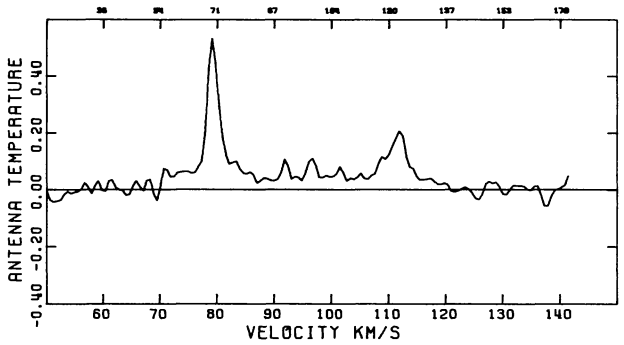

Figure 36 OH 9.9+0.4.

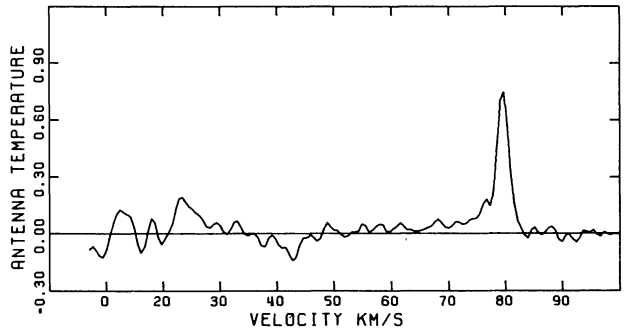

Figure 37 OH 10.0−0.1.

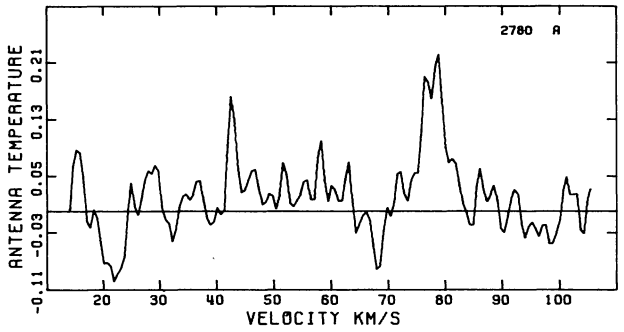

Figure 38 OH 10.4+0.0.

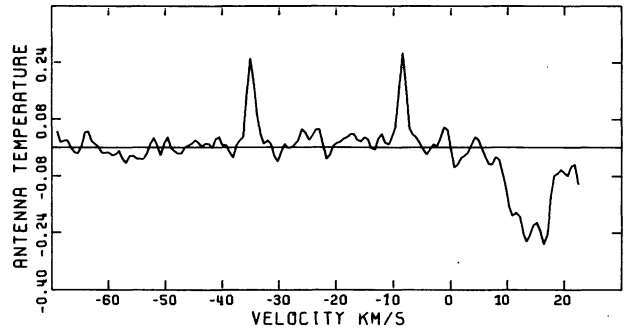

Figure 39 OH 11.1+0.0.

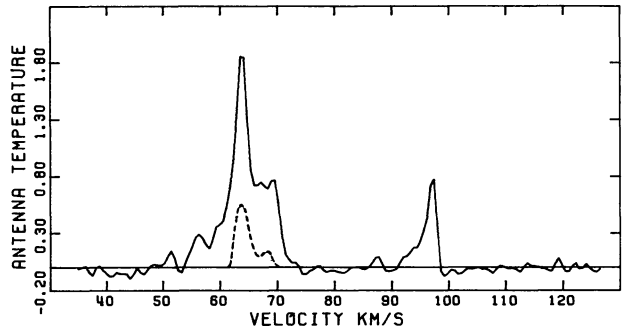

Figure 40 OH 11.3+0.0, dashed line represents the low-velocity component, that is obtained from the total profile (drawn) in a manner described in the text.

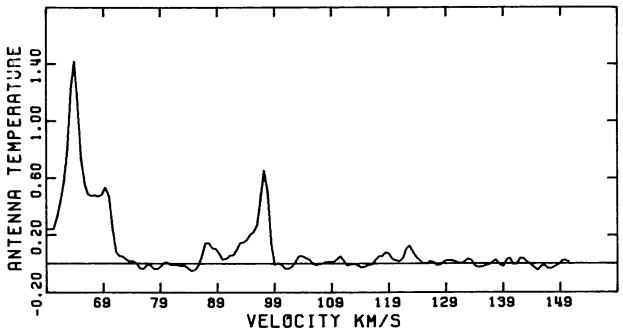

Figure 41 OH 11.4−0.1.

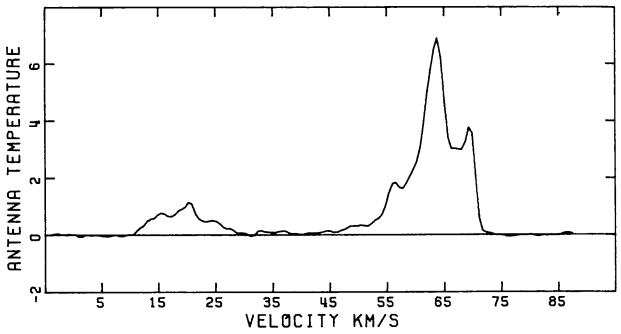

Figure 42 OH 11.5−0.1.

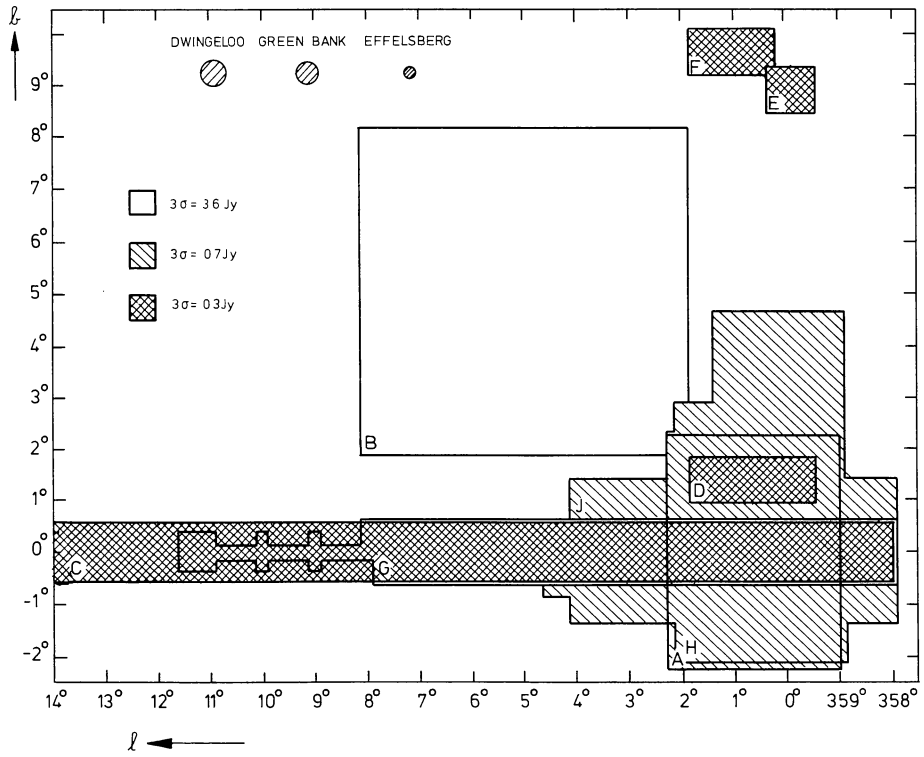

Figure 1 Extent of the surveyed areas. The hatched circles indicate the HPBW of the telescopes used. The squares depict the 3 σ sensitivities of the correspondingly marked areas.